

Minimally Actuated Transformation of Origami Machines

Fabio Zuliani, Chang Liu [✉], Jamie Paik [✉], and Samuel M. Felton [✉]

Abstract—Origami-inspired machines are a promising approach to robotic transformation. In this letter, we present a new method for transformation that uses dynamic response to change the mountain–valley fold pattern. We propose a dynamic model and validate it through experimental characterization of sample mechanisms. We demonstrate that these mechanisms reliably change their dynamic behavior at a discrete switching frequency, and this frequency can be changed by varying the stiffness and mass of the mechanism. This indicates that mechanisms can be designed to respond to different frequencies and selectively transform from a global input. We demonstrate a three-fingered gripping mechanism with a single actuator that can transform between four nontrivial configurations. We believe that this approach can be applied to several types of origami structures.

Index Terms—Dynamics, compliant joint/mechanism, grippers and other end-effectors, underactuated robots.

I. INTRODUCTION

ORIGAMI-INSPIRED engineering has many applications in robotics: it enables small and lightweight machines [1]–[3], it is cost effective and easy to manufacture [4]–[8], and it can produce machines that compress into a small volume [9]–[12]. One application particularly relevant to this letter is robotic transformation, in which the machine actuates its folded structure to transform between different shapes or functionalities. However, many origami robots rely on costly actuators distributed throughout the fold pattern to enable this transformation. Common examples include shape memory materials [13]–[15] and pneumatics [16], [17]. This increases the cost and complexity of a given design.

The theoretical basis for an origami pattern that can transform between multiple shapes is well established. Benbernou *et al.* discovered and demonstrated a ‘universal’ crease pattern that can form into a voxel approximation of any volume [18]. Most crease patterns can adopt multiple mountain-valley (MV) assignments from the flat-unfolded state, and these MV

Manuscript received September 10, 2017; accepted January 14, 2018. Date of publication January 31, 2018; date of current version February 22, 2018. This letter was recommended for publication by Associate Editor S. Briot and Editor P. Rocco upon evaluation of the reviewers’ comments. (Corresponding author: Samuel M. Felton.)

F. Zuliani, C. Liu, and S. M. Felton are with the College of Engineering, Northeastern University, Boston, MA 02115 USA (e-mail: fabzuliani@gmail.com; liu.chang7@husky.neu.edu; s.felton@northeastern.edu).

J. Paik is with the School of Engineering, Ecole Polytechnique Fédérale de Lausanne, Lausanne 1015, Switzerland (e-mail: jamie.paik@epfl.ch).

This letter has supplementary downloadable material available at <http://ieeexplore.ieee.org>, provided by the authors. The Supplemental Materials contain a video showing different origami mechanisms being actuated at different frequencies, and the resulting behavior. This material is 8.93 MB in size.

Digital Object Identifier 10.1109/LRA.2018.2800126



Fig. 1. An origami gripping system with three fingers in different configurations.

assignments usually result in different geometries and kinematic motion patterns [19], [20].

In contrast, studies into the dynamics of origami mechanisms are limited. Existing models approximate the crease pattern as an assembly of rigid linkages [21]–[24]. These are sufficient in most quasistatic conditions, but physical origami enters a kinematic singularity in the flat-unfolded state, and these models cannot predict the MV assignment of a crease pattern from the singularity. Individual mechanisms have been studied that harness the compliance of physical origami to transform [11], [25]–[28], including in nominally zero-degree-of-freedom (0-DOF) systems [29], [30], but these have not resulted in a unified model for physical origami.

In this letter we present a new approach to origami transformation that uses a single actuator to both control the fold angle and change the folding configuration. With this ability we can create kinematically constrained systems that transform between multiple kinematic configurations, making it a type of underactuated mechanism that is nevertheless capable of precise quasistatic motions. We present a dynamic model of the mechanism and relate it to the switching frequency at which transformation occurs. To demonstrate this concept we built and operated a multi-vertex Miura mechanism with a single actuator that can transform its shape to different tasks through dynamic actuation at specific frequencies (see Fig. 1). The ability to

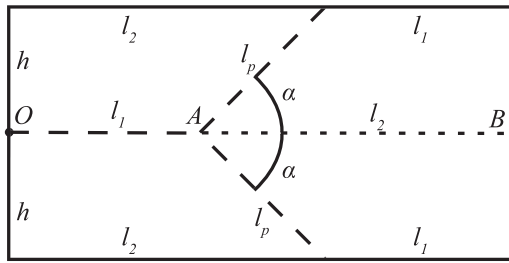


Fig. 2. The Miura fold pattern. l_1 , l_2 , and h define lengths of the edges, O , A , and B identify points on the mechanism, and α is the angle between the spinal (horizontal) and peripheral creases. Mountain folds are indicated by dashed lines and valley folds by dotted lines.

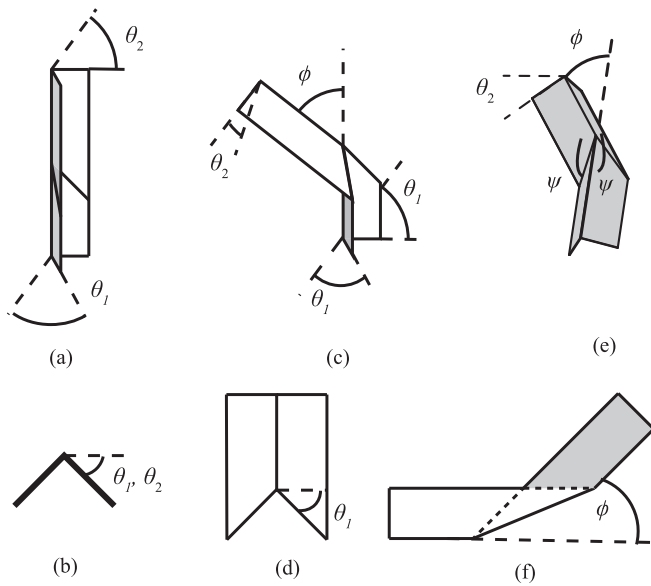


Fig. 3. Isometric (a) and top (b) views of the Miura fold in a parallel configuration where $\theta_1 = \theta_2$ are the spinal angles. Isometric (c), top (d), lower isometric (e), and side (f) views of the Miura fold in an anti-parallel configuration where $\theta_1 = -\theta_2$, ϕ is the angle between the upper and lower spinal hinges, and ψ is the folded angle of the peripheral hinges.

select the configuration of an origami mechanism through a single open-loop input is a novel capability. We applied this concept to a three-finger gripper with a single actuator that is capable of precise quasistatic motion and can transform its configuration to achieve multiple grasping patterns.

II. DESIGN

A. Origami Design

The elementary component of the system presented here is the Miura vertex. It is an origami pattern made of four plates connected by four creases (see Fig. 2) [8], [15]. The Miura pattern is well known as a proposed method for deploying satellites [9], and has a single kinematic DOF and two possible MV assignments. The two parallel creases (OA and AB) are the spinal creases with fold angles θ_1 and θ_2 and the other two are the peripheral creases with a folded angle ψ (see Fig. 3). These angles are equal to zero when the mechanism is flat. The Miura pattern can be folded into either a parallel configuration, defined as the configuration where $\theta_1 = \theta_2$ and $\phi = \psi = 0^\circ$, or

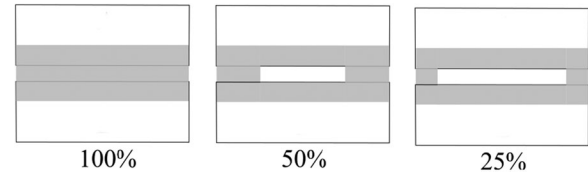


Fig. 4. The stiffness of each hinge can be varied by changing its total width. This is done by cutting out inner portions of the hinge.

an anti-parallel configuration where $\theta_1 = -\theta_2$ and ϕ and ψ are functions of θ_1 (see Fig. 3). Both configurations are symmetric across the spinal plane.

Each panel has a right-angle trapezoidal shape with a short horizontal edge of length l_1 and a long horizontal edge of length l_2 with a height h as shown in Fig. 2. The angle between the spinal and peripheral creases is α . Adjacent panels are connected with a 1-DOF rotational hinge. The lengths of our physical system are $h = 25.4$ mm, $l_1 = 40.6$ mm, $l_2 = 60.6$ mm, and $\alpha = 45^\circ$.

B. Physical Design

The mechanisms were fabricated using a laminate approach established in previous origami research [1], [4]. We selected 0.125 mm thick polystyrene sheets for the panels because it is sufficiently rigid while still being lightweight and machinable with a laser cutter. We used flexural hinges at each crease because they are easily fabricated and their stiffness can be tuned. Several combinations of flexible polymers and glues were investigated to find the most resilient material with a high repeatability in operation and fabrication. After experimental comparisons, we selected standard shipping tape (Scotch Heavy Duty Shipping Packaging Tape) because the adhesive layer was consistent across samples and did not require additional steps for curing. The tape was applied to one side of the polystyrene across the gaps between each pair of plates, so that only the tape connected the plates. The stiffness of these hinges is directly proportional to the width of the flexible joints, so it is easy to tune the stiffness of each hinge even after assembly by laser machining sections away, as shown in Fig. 4.

III. MODELING

We start by developing a 2nd-order dynamic model for each configuration (parallel and anti-parallel, Fig. 3) from the kinematics. We then propose that the system is a hybrid model that can discretely switch between configurations when passing through the flat-unfolded state. Finally, we propose that the switching behavior of the hybrid model is determined by the system parameters and actuation frequency, resulting in a repeatable configuration transformation based on the input frequency.

A. Direct Kinematic Model

We first calculate a lumped-parameter dynamic model for each configuration by solving for the kinematics of each hinge and plate with respect to the state variable θ_1 . We assume that

the origami structure is an assembly of rigid linkages (the plates) connected by revolute joints (the hinges), and that the mechanism stays in a single configuration. The inertia is derived from the mass of the plates and the system stiffness is due to the flexural hinges, which act like rotary springs. We then apply the Euler-Lagrange equations to solve for the equivalent inertia and stiffness in each configuration.

For these models, gravity is neglected. Our interest lies in the behavior of the mechanism at or near the flat-unfolded state, where the mechanism can switch its configuration. In this state, the mechanism is upright and the effect of gravity is negligible. In addition, we observed that the mechanism does not noticeably deflect when oriented in different directions, indicating that the hinge stiffness is substantially greater than the gravity force.

1) *Parallel Dynamics*: In the parallel configuration, the plates rotate around the spinal hinge [see Fig. 3(a) and (b)]. The inertial moment of each half around the spinal hinge I_θ is a function of h and the mechanism mass m . The stiffness k_θ of the spinal hinge is a function of l_1 , l_2 , the flexure thickness t , width w , and Young's modulus E . We solve for k_θ by considering the moment M_h of the flexural hinge as a function of curvature κ and area moment I_h .

$$M_h = EI_h\kappa = E \left(\frac{lt^3}{12} \right) \frac{\theta}{w} = k_\theta\theta \quad (1)$$

$$k_\theta = E \frac{(l_1 + l_2)t^3}{12w} \quad I_\theta = \frac{m}{2} \frac{h^2}{3} \quad (2)$$

Because $\phi = \psi = 0$ at all times, we can derive a second-order model for θ_1 , using the torque τ at the spinal hinge as an input.

$$\tau = 2I_\theta\ddot{\theta}_1 + 2k_\theta\theta_1 \quad (3)$$

$$= I_p\ddot{\theta}_1 + k_p\theta_1 \quad (4)$$

In this way we solve for the parallel stiffness k_p and parallel inertia I_p .

2) *Anti-Parallel Dynamics*: In the anti-parallel configuration [see Fig. 3(c)–(f)], the forward kinematics can be derived by treating each crease as a vector, as illustrated by Miyashita *et al.* [8]. Using this model, we can derive explicit kinematic equations for ϕ and ψ as functions of θ_1 and α .

$$\phi = 2 \arctan(\sin \theta_1 \tan \alpha) \quad (5)$$

$$\psi = \arccos(\sin^2 \theta_1 \cos \phi - \cos^2 \theta_1) \quad (6)$$

In this configuration the kinetic energy T is the sum of the energy T_θ due to the plates rotating around the spine at velocity $\dot{\theta}$ and the energy T_ϕ due to the upper segment rotating around the vertex with speed $\dot{\phi}$. The potential energy V is the sum of the energy V_θ due to the displacement of the spinal hinges θ and the energy V_ψ due to the displacement of the peripheral hinges ψ . If we consider that I_ϕ is the inertial moment of the two upper plates around the z-axis and k_ψ is the combined stiffness

TABLE I
TYPICAL SYSTEM PARAMETERS FOR A SINGLE-VERTEX MECHANISM WITH FULL-WIDTH HINGES AND NO ADDED MASS

Variable	Name	Value	Unit
Mechanism mass	m	14	g
Flexure thickness	t	78	μm
Flexure width	w	2	mm
Flexure Young's modulus	E	1.5	GPa
Spinal stiffness	k_θ	3.0	mN-m
Peripheral stiffness	k_ψ	2.0	mN-m
Spinal inertia	I_θ	1.5	$\text{mg}\cdot\text{m}^2$
Segment inertia	I_ϕ	15.9	$\text{mg}\cdot\text{m}^2$
Anti-parallel natural frequency	f_a	2.3	Hz
Parallel natural frequency	f_p	7.2	Hz
Hybrid natural frequency	f_h	3.5	Hz

of the peripheral hinges, then:

$$k_\psi = 2E \frac{l_p t^3}{12w} \quad I_\phi = m \left[\frac{l_1^2}{3} + \frac{3(l_2 - l_1)^2}{2} \right] \quad (7)$$

$$T_\theta = \frac{1}{2} (2I_\theta) \dot{\theta}_1^2 \quad T_\phi = \frac{1}{2} (I_\phi) \dot{\phi}^2 \quad (8)$$

$$V_\theta = \frac{1}{2} (2k_\theta) \theta_1^2 \quad V_\psi = \frac{1}{2} (k_\psi) \psi^2 \quad (9)$$

From the Lagrangian equations we can derive a second-order model for θ_1 .

$$L = T - V = (T_\theta + T_\phi) - (V_\theta + V_\psi) \quad (10)$$

$$= \left[I_\theta \dot{\theta}_1^2 + \frac{1}{2} (I_\phi) \dot{\phi}^2 \right] - \left[k_\theta \theta_1^2 + \frac{1}{2} (k_\psi) \psi^2 \right] \quad (11)$$

Solving the Euler-Lagrange equation leads to a lumped mass-spring model. We then linearize this around $\theta_1 = 0$ because our interest is in configuration switching, which happens at the flat-unfolded state. If $\alpha = 45^\circ$ like in our physical system, we can simplify to a single anti-parallel stiffness k_a and anti-parallel inertia I_a .

$$\tau = \left[2I_\theta + I_\phi \left(\frac{\partial \phi}{\partial \theta_1} \right)^2 \right] \ddot{\theta}_1 + \left[2k_\theta + k_\psi \left(\frac{\partial \psi}{\partial \theta_1} \right)^2 \right] \theta_1 \quad (12)$$

$$= (2I_\theta + 4I_\phi) \ddot{\theta}_1 + (2k_\theta + 4k_\psi) \theta_1 \quad (13)$$

$$= I_a \ddot{\theta}_1 + k_a \theta_1 \quad (14)$$


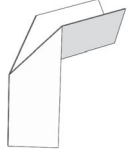


From this we can derive the natural frequencies in the parallel (f_p) and anti-parallel (f_a) patterns:

$$f_p = \frac{1}{2\pi} \sqrt{\frac{k_p}{I_p}} \quad (15)$$

$$f_a = \frac{1}{2\pi} \sqrt{\frac{k_a}{I_a}} \quad (16)$$

For a typical structure (full-width hinges for 100% stiffness and total mass $m = 0.014$ kg), this results in $f_a = 2.3$ Hz and $f_p = 7.2$ Hz. (see Table I).

TABLE II
TWO DYNAMIC PATTERNS—PAIRS OF BACKWARD AND FORWARD
CONFIGURATIONS—WERE OBSERVED IN THE SINUSOIDAL ACTUATION OF THE
MIURA MECHANISM

Pattern	Backward	Forward
#1		
#2		

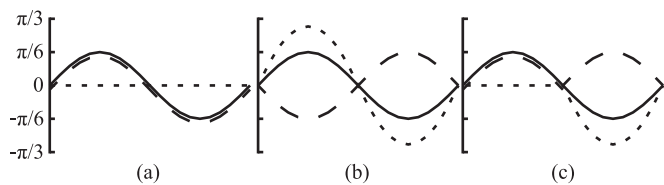


Fig. 5. Representative values of θ_1 (solid line), θ_2 (dashed line), and ϕ (dotted line) in the (a) parallel, (b) anti-parallel, and (c) hybrid dynamic patterns.

B. Hybrid Model

The origami mechanism has a kinematic bifurcation point when the system is in the flat-unfolded state. This allows for the system to switch between configurations as the state variable passes through the origin, resulting in three possible dynamic patterns: The system can remain in the parallel configuration on both sides of the origin [which we will refer to as the parallel dynamic pattern or pattern #2 (see Table II)], remain in the anti-parallel configuration (the anti-parallel dynamic pattern), or it can switch between the two, so that the configuration is parallel when $\theta_1 > 0$ and anti-parallel when $\theta_1 < 0$ (or vice versa), and θ_1 and θ_2 are continuous at $\theta_1 = 0$ (see Fig. 5). We refer to this as the hybrid dynamic pattern (or Pattern #1, Table II) because it can be described with a hybrid dynamic model. In the hybrid pattern, the system parameters exhibit a discrete change from the parallel to anti-parallel values (or vice-versa) each time $\theta_1 = 0$. This hybrid system has a natural period $p_h = p_p/2 + p_a/2$, where p_p and p_a are the natural periods of the parallel and anti-parallel systems. This results in a natural frequency f_h that falls between f_p and f_a . For our example, $f_h = 3.5$ Hz (see Table I).

C. Configuration-Switching Model

These models predict the dynamic behavior of the system assuming we know what dynamic pattern it is following, and therefore what configuration the mechanism will enter from the bifurcation point. However, they do not explicitly predict which

dynamic pattern it will follow. We use the term dynamic pattern to refer to the pair of configurations that a mechanism alternates between as it oscillates across the flat-unfolded state. In physical experiments we observed that the mechanisms exhibited one of two distinct dynamic patterns when driven by a sinusoidal input. The first (Pattern 1, Table II) consists of the mechanism alternating between the parallel and anti-parallel configurations as θ_1 crosses the origin. In the second (Pattern 2, Table II), the mechanism remains in the parallel configuration.

We first considered the possibility that the bifurcation could be driven by bias in the fold direction of θ_2 . However, we observed that the system would spontaneously enter both the parallel and anti-parallel configurations in either direction (Supplemental Video), so we discounted this explanation. Second, we considered if the rigid-body dynamics could predict the configuration. We would expect that in the flat-unfolded state there would be no spring forces and inertia would dominate the system. However, if inertia were the only factor, then the configuration would never switch because switching requires the upper segment (θ_2) to change directions at the flat position (see Fig. 5). Therefore, we would never see a hybrid pattern.

Instead we observed that the dynamic pattern (and therefore the configuration) depended on the actuation frequency. At low speeds, the upper segment angle θ_2 will tend to stay on one side of the origin (either positive or negative) while the lower segment switches, resulting in a reliable configuration change and a hybrid dynamic pattern. At higher frequencies, the kinetic energy of the upper segment is great enough to carry θ_2 across the origin so that θ_2 changes signs every time θ_1 does, resulting in a parallel pattern.

From these observations we propose that the switching frequency shares a similar relationship to the system parameters as the natural frequency — as the stiffness increases, the resistance to change increases, and a higher frequency is necessary to overcome that threshold. As the mass increases, the kinetic energy increases, so a lower speed (and frequency) is necessary to reach the threshold. Because of these correlations, we predict that the switching frequency is proportional to the natural frequency $f_{switching} \propto f_h$.

IV. EXPERIMENTS AND RESULTS

A. Single Vertex Miura Fold

The experimental tests were performed with a setup ensuring θ_1 is actuated symmetrically across the spinal plane (see Fig. 6). The testing fixture consisted of a motor (Uxcell 12V motor with gearbox) coupled with a rotary-to-linear mechanism made of acrylic sheets cut with a laser and linked together with acrylic glue and aluminum barrel hinges. The input signal is sinusoidal with an amplitude $\theta_{1,max} = 30^\circ$.

In our first set of experiments, three mechanisms with different hinge stiffnesses ($k_a = 4.7$ mN-m, 9.3 mN-m, or 14 mN-m) were actuated by a sinusoidal input with a slowly increasing frequency (see Fig. 7) from 0 Hz to 4 Hz and the dynamic pattern was recorded as a function of frequency. The results show that there is a frequency threshold at which the dynamic pattern changes in a reliable manner, and this threshold depends on the

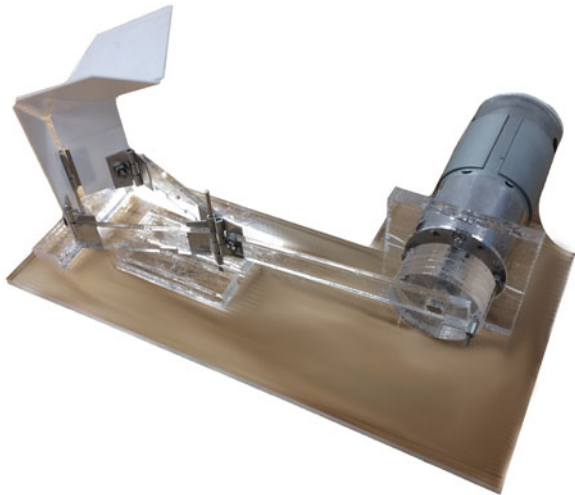


Fig. 6. The experimental mechanisms were driven by an electric motor through a transmission to sinusoidally fold the spine, resulting in θ_1 oscillating between 30° and -30° .

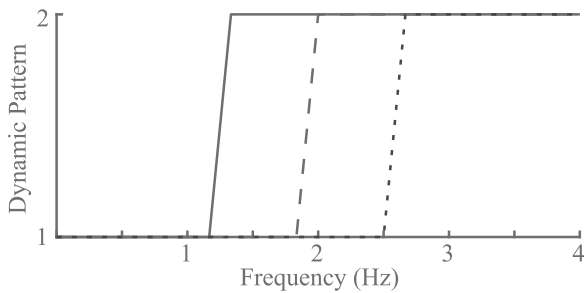


Fig. 7. Dynamic Pattern of the Miura mechanism as a function of frequency. The mechanism has a distinct switching frequency that varies with system stiffness. The solid line indicates a system with anti-parallel stiffness $k_a = 4.7$ mN-m, the dashed line is a system with $k_a = 9.3$ mN-m, and the dotted line is a system with $k_a = 14$ mN-m. The patterns are displayed in Table II.

system stiffness. This behavior can be seen in the Supplemental Video, and the patterns are shown in Table II.

We then built a single mechanism and progressively reduced the stiffness of its hinges by removing hinge material (see Fig. 4). In between each stiffness reduction we placed the mechanism in the flat-unfolded state and applied a frequency sweep while recording the dynamic pattern. We then identified the switching frequency as the point when the dynamic pattern changed from a Pattern #1 to Pattern #2 (see Fig. 8). This was repeated 10 times for each stiffness. These results indicate that as the stiffness increases, the switching frequency increases.

In order to show repeatability across mechanisms, we performed the same test but with different samples made from the same design (see Fig. 9) and stiffness values ranging from 16% to 100% of the maximum system stiffness. The switching frequency from one pattern to the other (see Table II) was recorded for four samples with three trials per sample for an overall $N = 12$. These results match our previous observations, but indicate that there is noticeable variation between different mechanisms.

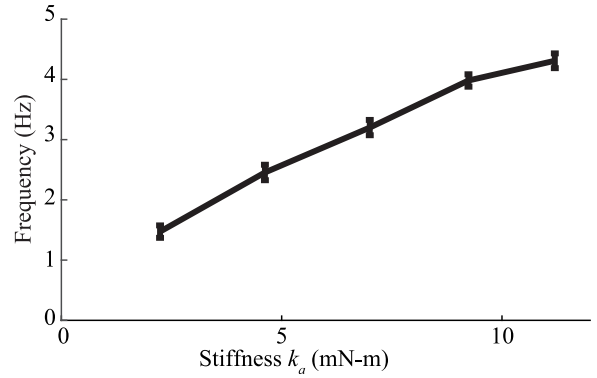


Fig. 8. Switching frequencies between the two dynamic patterns are plotted as a function of the anti-parallel stiffness k_a of the single vertex Miura mechanism. Error bars indicate standard deviation, $N = 10$.

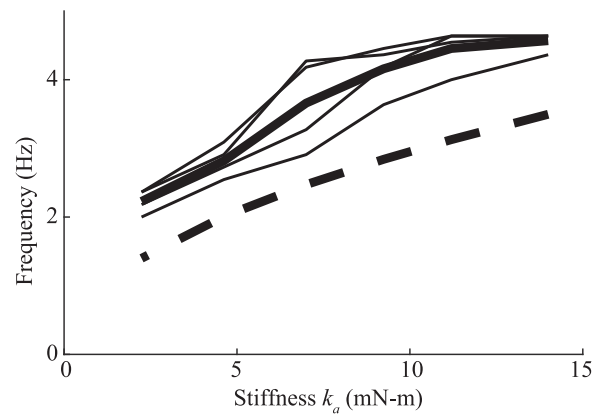


Fig. 9. Plot of the switching frequency as a function of the anti-parallel stiffness k_a . The thin solid lines indicate the switching frequency from experimental trials of single mechanisms, and the thick line is their average. The dashed line represents the hybrid natural frequency f_h .

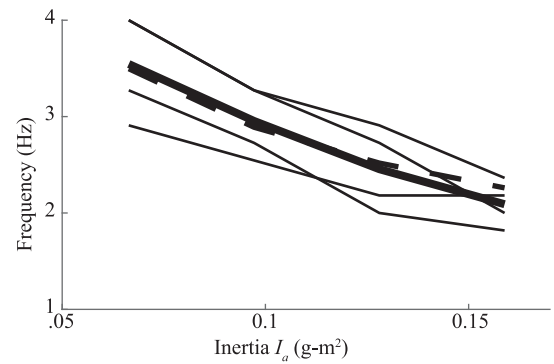


Fig. 10. Plot of the switching frequency as a function of the anti-parallel inertia I_a . The thin solid lines indicate the switching frequency from experimental trials of single mechanisms, and the thick line is their average. The dashed line represents the hybrid natural frequency f_h .

We then varied the mass of the upper panels between 14 g to 34 g by adding additional layers to the panels (see Fig. 10). The switching frequency from dynamic pattern #1 to #2 was recorded for four samples with three trials per sample. These results indicate that as the system inertia increases, the switching frequency decreases.

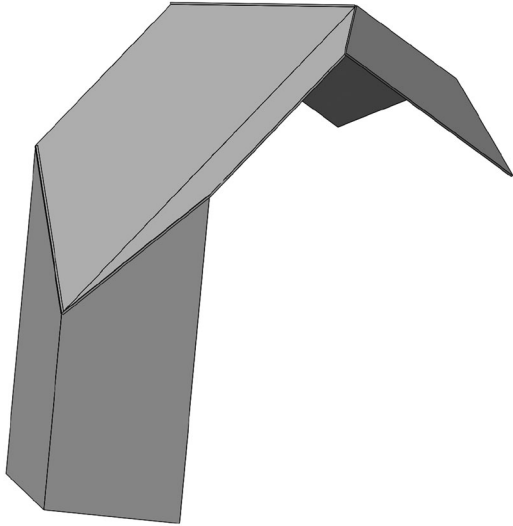


Fig. 11. The two-vertex Miura mechanism was used as a finger to design the origami hand.

In Figs. 9 and 10 we include f_h (dashed line), which demonstrates a proportional relationship with the switching frequency. In Fig. 9 the hybrid frequency is on average 24% lower than the switching frequency, indicating that the two frequencies are proportional but not equal. In Fig. 10 they do match closely; combined with the previous results, this suggests that there are other factors affecting the switching frequency that we have not accounted for.

B. Two-Vertex Miura Fold

We extended this concept to create an origami finger with two vertices (see Fig. 11). This structure still has a single degree of freedom but now has four different configurations (Supplemental Video). To demonstrate that selective transformation of multiple vertices is possible, we built an origami finger and characterized it through oscillatory inputs. The dynamic patterns we observed are listed in Table III.

The dynamic pattern was recorded as a function of actuation frequency in fingers with three different system stiffnesses (see Fig. 12). The 100% stiff finger predominantly stays in three different patterns depending on the actuation frequency. The 50% stiff finger exhibits the same general trend but is less predictable, and at four hertz returns to pattern #4. A third sample was built with a 100% stiff lower vertex and a 50% stiff upper vertex. It demonstrated a more complex behavior but reaches a #6 pattern at a slightly lower frequency than the stiffer model and maintains it up to five hertz.

The proportion of time the mechanism spent in each dynamic pattern was measured as a function of frequency (see Fig. 13). At each frequency, the mechanism oscillated twenty times and the pattern was recorded each period. These results reveal how reliable the pattern is for a given open-loop signal, and the data indicates that high and low frequency-actuation results in predictable dynamic patterns, but between 1.5 Hz and 2.5 Hz, the pattern is not predictable and could end up in three different patterns.

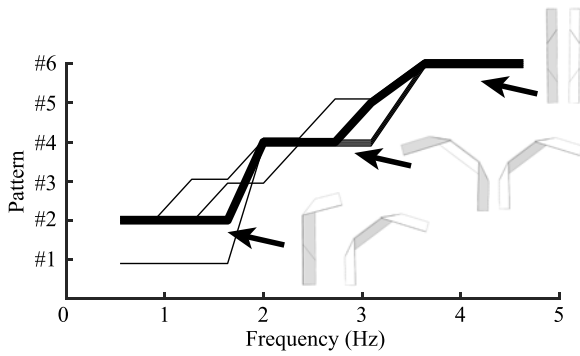
TABLE III
SIX DYNAMIC PATTERNS WERE OBSERVED DURING SINUSOIDAL ACTUATION OF THE TWO-VERTEX MECHANISM

Pattern	Backward	Forward
#1		
#2		
#3		
#4		
#5		
#6		

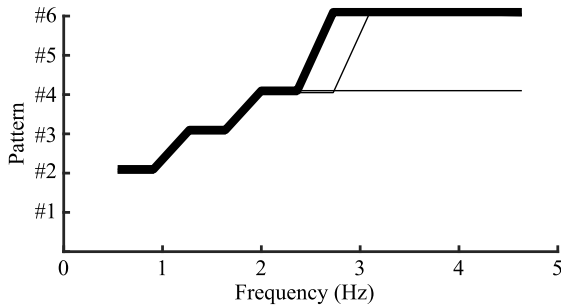
C. Gripping System

A gripping system consisting of three origami fingers was built and actuated by a single motor with a rotary-to-linear transmission. The three fingers were built with stiffnesses equal to 25%, 50% and 100% of the maximum stiffness (corresponding to uncut hinges) in order to obtain a different behavior for each of the fingers at a given actuation frequency. This enables us to selectively transform fingers by applying frequencies which correspond to transformation in one finger but not the others (Supplemental Video).

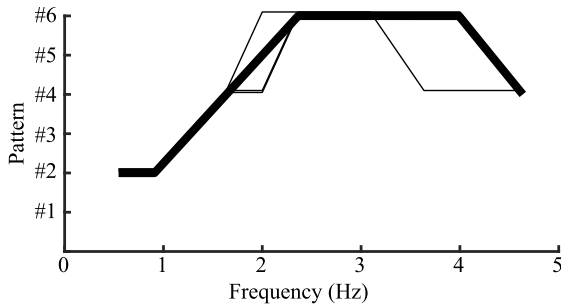
Fig. 14 shows the percentage of time each finger spends in each dynamic pattern as a function of frequency and shows that we can select a configuration of a set of fingers depending



(a)



(b)



(c)

Fig. 12. Dynamic pattern of a two-vertex mechanism as a function of actuation frequency with (a) a maximum system stiffness (100%) (b) a reduced upper-vertex stiffness of 50% and a lower-vertex stiffness of 100%, and (c) an overall reduced stiffness of 50% at both vertices. (four samples, thick line for the most likely pattern).

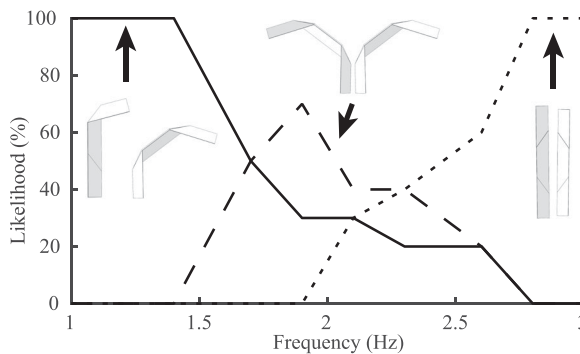


Fig. 13. The percentage of time the two-vertex mechanism spent in each dynamic pattern as a function of frequency, indicating the repeatability at that frequency. Solid line indicates pattern #2, dashed line indicates pattern #4, and dotted line indicates pattern #6.

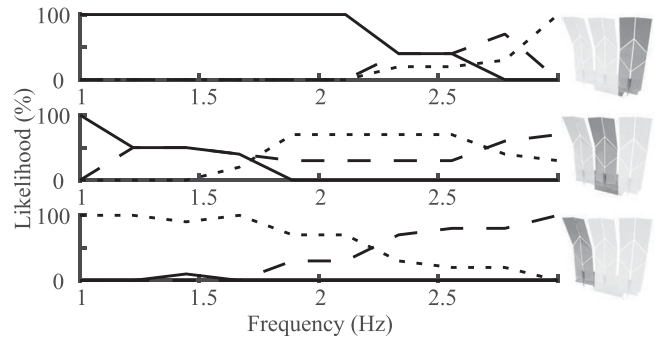


Fig. 14. The likelihood of exhibiting a particular dynamic pattern at each frequency for three fingers actuated simultaneously with a single actuator. Each line represents a pattern: Solid line for #2, dashed line for #4, and dotted line for #6. Top graph is for finger at 100% stiffness, middle is for 50% stiffness, and bottom is for 25% stiffness.

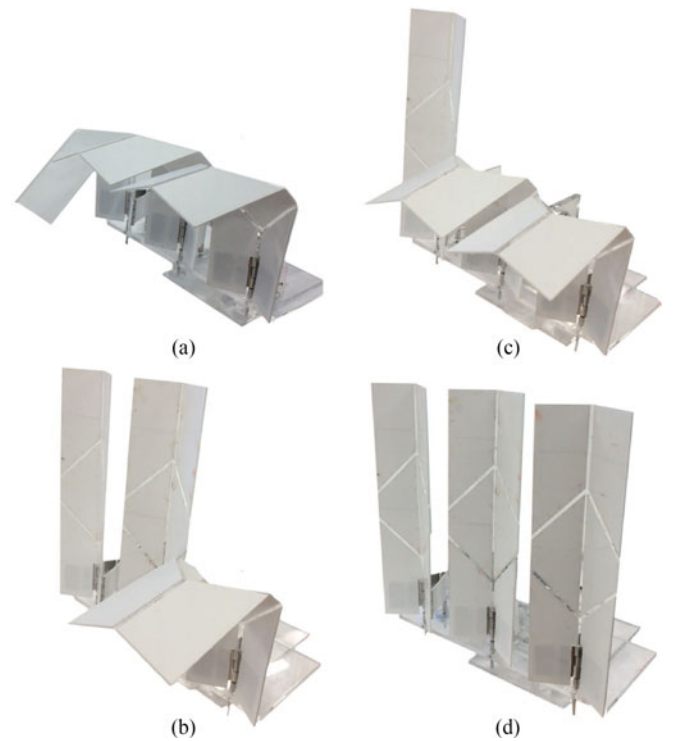


Fig. 15. Different configurations of the three fingers gripping system that are reached reliably with a respective stiffness of 25%, 50% and 100% for the fingers from left to right at frequencies of (a) 0.8 Hz (b) 1 Hz (c) 2 Hz and (d) 3 Hz.

only on the frequency of actuation with a single actuator for the whole system. Fig. 15 shows the different configurations reached with different frequencies between 0.8 and 3 Hz in a reliable manner. These results validate the concept of using particular frequencies to induce desired configuration changes in an origami mechanism.

V. DISCUSSIONS AND CONCLUSIONS

In this letter we demonstrated that mechanisms can demonstrate discretely different dynamic patterns when actuated above or below a particular switching frequency, and that this

can be used to induce a kinematic transformation. Furthermore, we showed that the switching frequency is dependent on system parameters and proposed a relationship between switching and the natural frequency. An origami hand demonstrated that a single actuator can repeatably induce transformation between multiple kinematic states. In total, these results indicate that origami mechanisms can be tuned through their mass and stiffness to enter specific configurations at specific frequencies, providing a method for controllable transformation through dynamic excitation.

We observed limitations to implementing this transformation in physical systems. If the actuation frequency is mechanically programmed via stiffness and mass, it will be coupled to other design parameters. Most notably, with multiple elements that are individually controlled, differentiating the vertices requires that some hinges are a fraction as stiff as others, limiting the stiffness of the entire structure. Future work should address some way to decouple or mitigate the effect of reduced stiffness and increased mass on the device operation while still enabling multiple actuation frequencies.

There is also further research necessary to fully model the underlying physics of configuration switching. The results indicate that there are additional parameters besides stiffness and inertia that affect switching frequency. Future dynamic experiments should include impulse, step, and periodic bang-bang inputs to better characterize the system, and identify how the system configuration affects pattern switching. Quasistatic load tests should characterize the stiffness of the system as a whole to identify coupling between the hinges and plate compliance. The results also indicate that transformation is not always predictable. This approach could be improved through feedback control, which may be able to address the repeatability issues. Finally, these results should be generalized to other fold patterns in order to establish a unified approach to origami transformation.

REFERENCES

- [1] P. S. Sreetharan, J. P. Whitney, M. D. Strauss, and R. J. Wood, "Monolithic fabrication of millimeter-scale machines," *J. Micromech. Microeng.*, vol. 22, no. 5, 2012, Art. no. 055027.
- [2] W. Fischer, G. Caprari, R. Siegwart, I. Thommen, W. Zesch, and R. Moser, "Foldable magnetic wheeled climbing robot for the inspection of gas turbines and similar environments with very narrow access holes," *Ind. Robot. Int. J.*, vol. 37, no. 3, pp. 244–249, 2010.
- [3] M. Salerno, K. Zhang, A. Menciassi, and J. S. Dai, "A novel 4-DOF origami grasper with an SMA-actuation system for minimally invasive surgery," *IEEE Trans. Robot.*, vol. 32, no. 3, pp. 484–498, Jun. 2016.
- [4] S. Felton, M. Tolley, E. Demaine, D. Rus, and R. Wood, "A method for building self-folding machines," *Sci. Mag.*, vol. 345, no. 6197, pp. 644–646, 2014.
- [5] L. Dufour, K. Owen, S. Mintchev, and D. Floreano, "A drone with insect-inspired folding wings," *IEEE/RSJ Int. Conf. Intell. Robots Syst.*, 2016, pp. 1576–1581.
- [6] H. Shigemune, S. Maeda, Y. Hara, N. Hosoya, and S. Hashimoto, "Origami robot: A self-folding paper robot with an electrothermal actuator created by printing," *IEEE/ASME Trans. Mechatronics*, vol. 21, no. 6, pp. 2746–2754, Dec. 2016.
- [7] H. Shigemune, S. Maeda, Y. Hara, and S. Hashimoto, "Printed paper robot driven by electrostatic force," in *Proc. IEEE/RSJ Int. Conf. Intell. Robots Syst.*, 2014, pp. 536–541.
- [8] S. Miyashita, C. D. Onal, and D. Rus, "Multi-crease self-folding by global heating," *Artif. Life*, vol. 21, pp. 398–411, 2015.
- [9] K. Miura, "Method of packaging and deployment of large membranes in space," *Ins. Space Astronaut. Sci.*, Sagamihara, Japan, Rep. 618, 1985.
- [10] J. Cai, X. Deng, J. Feng, and Y. Zhou, "Geometric design and mechanical behavior of a deployable cylinder with Miura origami," *Smart Mater. Struct.*, vol. 24, no. 12, 2015, Art. no. 125031.
- [11] S.-M. Baek, D.-Y. Lee, and K.-J. Cho, "Curved compliant facet origami-based self-deployable gliding wing module for jump-gliding," in *Proc. ASME Int. Des. Eng. Tech. Conf. Comput. Inf. Eng. Conf.*, 2016.
- [12] M. Salerno, A. Firouzeh, and J. Paik, "A low profile electromagnetic actuator design and model for an origami parallel platform," *J. Mech. Robot.*, vol. 9, 2017, Art. no. JMR-16-1214.
- [13] D.-Y. Lee, J.-S. Kim, S.-R. Kim, J.-J. Park, and K.-J. Cho, "Design of deformable-wheeled robot based on origami structure with shape memory alloy coil spring," in *Proc. 10th Int. Conf. Ubiquitous Robots Ambient Intell.*, 2013, pp. 120–120.
- [14] S. M. Felton, K. P. Becker, D. M. Aukes, and R. J. Wood, "Self-folding with shape memory composites at the millimeter scale," *J. Micromech. Microeng.*, vol. 25, no. 8, 2015, Art. no. 085004.
- [15] A. Firouzeh and J. Paik, "An under-actuated origami gripper with adjustable stiffness joints for multiple grasp modes," *Smart Mater. Struct.*, vol. 26, no. 5, pp. 1–10, 2017.
- [16] X. Sun, S. M. Felton, R. J. Wood, and S. Kim, "Printing angle sensors for foldable robots," in *Proc. IEEE/RSJ Int. Conf. Intell. Robots Syst.*, 2015, pp. 1725–1731.
- [17] C. Liu and S. M. Felton, "A self-folding robot arm for load-bearing operations," in *Proc. IEEE/RSJ Int. Conf. Intell. Robots Syst.*, 2017, pp. 1979–1986.
- [18] N. M. Benbernou, E. D. Demaine, M. L. Demaine, and A. Ovadya, "Universal hinge patterns to fold orthogonal shapes," in *Origami5: Proc. 5th Int. Conf. Origam. Sci., Math. Edu.*, 2010, pp. 405–420.
- [19] Z. Abel *et al.*, "Rigid origami vertices: Conditions and forcing sets," *J. Comput. Geom.*, vol. 7, no. 1, pp. 171–184, 2016.
- [20] X. Liu, J. M. Gattas, and Y. Chen, "One-DOF superimposed rigid origami with multiple states," *Sci. Rep.*, vol. 6, 2016, Art. no. 36883.
- [21] E. D. Demaine and J. O'Rourke, *Geometric Folding Algorithms*. Cambridge, U.K.: Cambridge Univ. Press, 2007.
- [22] J. Cai, X. Deng, Y. Xu, and J. Feng, "Geometry and motion analysis of origami-based deployable shelter structures," *J. Struct. Eng.*, vol. 141, no. 10, 2015, Art. no. 06015001.
- [23] J. Cai, Z. Qian, C. Jiang, J. Feng, and Y. Xu, "Mobility and kinematic analysis of foldable plate structures based on rigid origami," *J. Mech. Robot.*, vol. 8, no. 6, 2016, Art. no. 064502.
- [24] L. Bowen, B. Trease, M. Frecker, and T. Simpson, "Dynamic modeling and analysis of an origami-inspired optical shield for the starshade spacecraft," in *Proc. ASME Conf. Smart Mater., Adapt. Struct. Intell. Syst.*, 2016, pp. 1–11.
- [25] S. M. Felton, D.-Y. Lee, K.-J. Cho, and R. J. Wood, "A passive, origami-inspired, continuously variable transmission," in *Proc. Int. Conf. Robot. Autom.*, 2014, pp. 2913–2918.
- [26] J. Cai, X. Deng, Y. Zhou, J. Feng, and Y. Tu, "Bistable behavior of the cylindrical origami structure with Kresling pattern," *J. Mech. Des.*, vol. 137, no. 6, 2015, Art. no. 061406.
- [27] J. Cai, X. Deng, Y. Zhang, J. Feng, and Y. Zhou, "Folding behavior of a foldable prismatic mast with Kresling origami pattern," *J. Mech. Robot.*, vol. 8, no. 3, 2016, Art. no. 031004.
- [28] J. Cai, Y. Liu, R. Ma, J. Feng, and Y. Zhou, "Nonrigidly foldability analysis of Kresling cylindrical origami," *J. Mech. Robot.*, vol. 9, no. 4, 2017, Art. no. 041018.
- [29] N. P. Bende *et al.*, "Geometrically controlled snapping transitions in shells with curved creases," *Proc. Nat. Acad. Sci.*, vol. 112, no. 36, pp. 11175–11180, 2015.
- [30] J. L. Silverberg *et al.*, "Origami structures with a critical transition to bistability arising from hidden degrees of freedom," *Nature Mater.*, vol. 14, no. 4, pp. 389–393, 2015.